coatings

MDPI

Article

Impact of Tungsten Incorporation on the Tribomechanical Behavior of $AlCrW_xSiN$ Films at Room and Elevated Temperature

Wolfgang Tillmann, Alexander Fehr * and Dominic Stangier

Institute of Materials Engineering, TU Dortmund University, Leonhard-Euler-Straße 2, 44227 Dortmund, Germany; wolfgang.tillmann@tu-dortmund.de (W.T.); dominic.stangier@tu-dortmund.de (D.S.)
* Correspondence: alexander.fehr@tu-dortmund.de; Tel.: +49-(0)231-755-5132

Abstract: $AlCrW_xSiN$ thin films ($0 \leq x \leq 17.1$ at.%) were synthesized by means of a hybrid magnetron sputtering process, merging direct current (DC) as well as tungsten high power impulse magnetron sputtering (HiPIMS) supplies. The influences of increasing the tungsten contents on the structural as well as the friction and wear behavior at room and high temperatures (500 °C) were elaborated. As a reference, a $W_{61.4}N_{38.6}$ system served to analyze synergetic effects on the oxidation behavior. Increased tungsten contents in $AlCrW_xSiN$ resulted in more distinctive (200)-, (202)-, and (311)-crystal orientations. A W/Cr ratio of ~1 could be correlated with a denser film growth, the highest hardness (24.3 ± 0.7 GPa), and a significantly decreased wear coefficient (<0.3 × 10^{-5} mm^3/Nm). Tribological tests performed at room temperature revealed that the coefficient of friction decreased with higher tungsten contents to μ~0.35. In contrast, at elevated temperatures, the coefficient of friction increased with higher W concentrations due to spotty oxidations in the wear track, which resulted in a locally increased surface roughness. Finally, a phase transformation of the WN film to m-WO_3 did not contribute to a friction reduction at 500 °C.

Keywords: chromium-based nitride; tungsten nitride; reactive magnetron sputtering; hybrid process; high temperature tribology

check for updates

Citation: Tillmann, W.; Fehr, A.; Stangier, D. Impact of Tungsten Incorporation on the Tribomechanical Behavior of $AlCrW_xSiN$ Films at Room and Elevated Temperature. *Coatings* **2021**, *11*, 1033. https://doi.org/10.3390/coatings11091033

Academic Editor: Kevin Plucknett

Received: 14 July 2021
Accepted: 25 August 2021
Published: 27 August 2021

Publisher's Note: MDPI stays neutral with regard to jurisdictional claims in published maps and institutional affiliations.

Copyright: © 2021 by the authors. Licensee MDPI, Basel, Switzerland. This article is an open access article distributed under the terms and conditions of the Creative Commons Attribution (CC BY) license (https://creativecommons.org/licenses/by/4.0/).

1. Introduction

The incorporation of tungsten within chromium-based nitrides offers various advantages such as an enhanced mechanical and tribological properties that extend the lifetime of cutting and forming tools. The reason for an increased hardness can be attributed to a refinement of the crystallite size [1] as well as to the formation of covalent bondings in WN, which forms as a second W_xN_y phase aside from CrN [2–4]. By varying the W content from 2 to 46 at.%, Chen et al. demonstrated an increase in nanohardness from 10.8 to 27.1 GPa. Hones et al. showed that $Cr_{1-x}W_xN$ films with $0.1 \leq x \leq 0.8$ exhibited a significantly higher hardness (24–29 GPa) when compared to binary CrN (13 GPa) [4]. With regard to the crystallographic properties, the crystal orientation changes from (111) to (200) with a higher W concentration, while maintaining an *fcc* structure [4–6]. Increasing tungsten concentrations further changes the film morphology from columnar to a fine-grained structure, resulting in a linear increase of the compressive stresses [4]. Besides doping CrN with tungsten, alloying with aluminum and silicon has also been established as a method for the synthesis of hard and thermally stable AlCrSiN films [7–9].

Several studies have exploited these alloying effects by synthesizing $CrAlSiN/W_2N$ superlattice structures with a hardness up to 40.3 GPa, which is based on a solid solution strengthening mechanism and a nanolayered coating structure [10,11], resulting in increased wear resistance [12]. In our recent studies, we have investigated the sputtering of AlCrSiWN using targets that include all coating constituents. In particular, the inert sputtering behavior of tungsten became obvious within these studies [13,14], since the

crystallization of W_xN_y is complex based on the transformations of α-W to *fcc* W_2N and to *hex* WN [15]. This behavior, however, can be influenced by HiPIMS processes with adaptions of the magnetic field strength and the pulsing configuration supporting the growth of dense tungsten nitrides [16]. Wu et al., for instance, employed a co-sputtering process employing HiPIMS and DC to synthesize nanostructured $Ti_{0.40}Al_{0.27}W_{0.33}N$ films. They showed that a bombardment with comparatively high-energetic W^+ ions, which were generated using an HiPIMS source, remarkably contributed to a densification of TiAlN films [17]. One reason for this can be found in the increased ionization and energy of W^+ provided by HiPIMS when compared to DC [18].

Based on these findings, this study aims at integrating a W HiPIMS source in a DC magnetron sputtering process to investigate the effects of different average HiPIMS powers on the structural and tribological properties of $AlCrW_xSiN$ films. In particular, the integration of tungsten is supposed to modify the microstructural properties of the films [18,19], thus leading to denser film growth. Although the tribological behavior of AlCrWSiN systems is partly explored [11,20], findings concerning the influence of tungsten on tribological performance at high temperature are still restricted. To elaborate the high temperature behavior of AlCrWSiN for hot working applications, future research is required. For this reason, particular emphasis will be placed on the tribological behavior at 500 °C with regard to the influence of tungsten on the oxidation behavior. In this context, the mechanical properties and the film adhesion are further investigated.

2. Experimental

2.1. Materials and Methods

As a substrate material for the $AlCrW_xSiN$ films, a hot work steel AISI H11 (1.2343, see Table 1) with a cylindrical dimension (Ø = 40 mm, t = 4 mm) was used. The substrates were previously vacuum hardened and annealed to obtain a hardness of 50 ± 1 HRC. Lapping (9 µm) and polishing processes with diamond suspension (3 µm) were conducted to obtain a substrate roughness of Ra = 2.3 ± 0.1 nm. The roughness was measured by means of a confocal white light interferometer MSurf, Nanofocus, Germany. After every polishing step and prior to the film deposition, all substrates were cleaned for 15 min in ethanol with the help of an ultrasonic bath.

Table 1. Chemical composition (wt.%) of the AISI H11 substrate [21].

C	Si	Mn	Cr	Mo	V	Fe
0.38	1.0	0.4	5.3	1.3	0.4	rest

The film depositions were conducted by means of magnetron sputtering in an industrial CC800/9 Custom, CemeCon AG, Germany PVD device, which was equipped with four DC cathodes and two HiPIMS cathodes. All utilized targets had a rectangular shape (500 mm × 88 mm). Prior to the coating deposition, the substrates were heated to a temperature of approximately 400 °C at a starting pressure of 10 mPa. Subsequently, argon ion etching was performed at a constant Ar pressure of 350 mPa and a MF-pulsed bias voltage of −650 V was applied to the substrates at a frequency of 240 kHz for 20 min to remove oxides from the targets and substrates. Furthermore, HiPIMS metal ion etching (MIE) was conducted by means of a chromium target applying an average power of 3.5 kW at a frequency of 500 Hz and an Ar controlled pressure of 355 mPa. MIE was performed for 30 min, applying an HiPIMS substrate bias of −1000 V to increase film adhesion.

During the $AlCrW_xSiN$ film depositions, the substrate table was rotated at 1 rpm. As shown in Table 2, the gas flow was set as Ar = 120 sccm and Kr = 80 sccm (Ar + Kr = 200 sccm) and the working pressure of 500 mPa was controlled by nitrogen, resulting in a N_2 flow of ~320 sccm. Furthermore, a DC bias voltage of −120 V was applied to the substrates and the deposition time for all films was 250 min. Two AlCr24 targets (each 5 kW), one Cr target (1 kW), and one silicon target (2 kW) were operated constantly in a DC mode in all film depositions. This target setup was adapted from our previous studies [22,23]. The

additional chromium target served to obtain an Al/Cr ratio of approximately 1. For the investigation of different tungsten contents in the $AlCrW_xSiN$ films, the average HiPIMS power on the W target was varied from 0 to 4 kW by a successive increase of 1 kW, while the frequency of 1 kHz and the pulse length of 100 µs were kept constant. Thus, one AlCrSiN film was synthesized according to previous studies [22,23] to systematically study the influence of increasing tungsten contents on the microstructural and tribological properties. Furthermore, a pure W_xN_y film was deposited by means of HiPIMS (3 kW) to analyze synergetic effects concerning the oxidative properties of the tungsten incorporation in $AlCrW_xSiN$.

Table 2. Deposition parameters of the films.

Ar/Kr Flow		**120 sccm/80 sccm**					
Pressure		**500 mPa, N_2 Controlled (N_2 Flow: ~320 sccm)**					
Heating Power		**5 kW (Substrate Temperature: ~400 °C)**					
Bias		**−120 V**					
Target	**Mode**	**(Average) Cathode Power [kW]**					
2 × AlCr24	DC	5	5	5	5	5	0
1 × Cr	DC	1	1	1	1	1	0
1 × Si	DC	2	2	2	2	2	0
1 × W	HiPIMS	0	1	2	3	4	3

2.2. Material Characterization

The microstructural analyses as well as the determinations of the chemical composition were conducted directly after the film deposition with the help of a field emission scanning electron microscope (SEM), FE-JSEM 7001F, Jeol, Tokyo, Japan, equipped with energy-dispersive X-ray spectroscopy (EDS) from Oxford Instruments (Abingdon, UK). Crystallographic investigations were made by means of a diffractometer D8 Advance, Bruker, Billerica, MA, USA, employing Co-Kα radiation with a wavelength of $\lambda = 0.179$ nm. A voltage of 40 kV and a current of 40 mA were set for all investigations.

Annealing of the $AlCrW_xSiN$ films was carried out in muffle furnace N100, Nabertherm, Lilienthal, Germany, at a heating rate of 10 K/min and a dwell time of two hours at 500 °C in atmosphere. For the determination of the microhardness as well as the Young's modulus of the as-deposited and annealed films, a nanoindenter G200, Agilent Technology, Santa Clara, CA, USA, was utilized according to the method of Oliver and Pharr [24]. The measurement included 49 indentations in a square area having a distance of 50 µm to each other and a poisson ratio of $\nu = 0.25$. For the exclusion of substrate influences, the hardness and elastic modulus were only evaluated in the upper 10% of the film thickness. The adhesion of the $AlCrW_xSiN$ films was examined by means of a scratch tester Revetest CSM Instruments (Peseux, Switzerland) applying a Rockwell C diamond tip with R = 200 µm. This tip produced three scratches, each of 10 mm in length with a linearly increasing force up to 100 N [25].

For the investigation of the tribological properties of the non-annealed samples at room temperature (RT) and 500 °C, a ball-on-disc test from CSM Instruments (Peseux, Switzerland) was employed. The tribometer included a heated table, upon which the cylindrical samples were mounted, and a thermocouple was used to control the substrate temperature. Each temperature level included three specimens to provide a statistical evaluation. A substrate temperature of 500 °C was chosen in order to avoid the deterioration of the mechanical properties of the AISI H11 (1.2343) substrates, since temperatures >500 °C induce a hardness decrease according to the tempering diagram of the steel. Al_2O_3 balls with a diameter of 6 mm were used as a counterpart and a linear velocity of 40 cm/s was set while applying a normal force of 10 N. The wear track had a radius of 11 mm and the sample was rotated 5000 times. The coefficient of friction (COF) was recorded in dependence of the sliding distance, which was the basis for the calculation of the average COF. For the determination of the wear volume, the optical 3D profilometer Infinite Focus

(Alicona Imaging GmbH, Raaba, Austria) was used by examining four different positions of each sample to calculate an average wear coefficient. In addition to this, the wear behavior was investigated by means of SEM and EDS to analyze tribochemical reactions.

3. Results and Discussion

3.1. Chemical Composition and Crystal Structure

From Figure 1 it can be concluded that an increasing HiPIMS power on the W target increased the tungsten contents (7.1–17.1 at.%) in the films. Similar results were reported by Lin et al., who synthesized WCrN films by means of dual-gun co-sputtering of Cr and W targets. They correlated the increased W contents with a proportional sputtering energy that is enabled by increased pulse powers on the tungsten target [2].

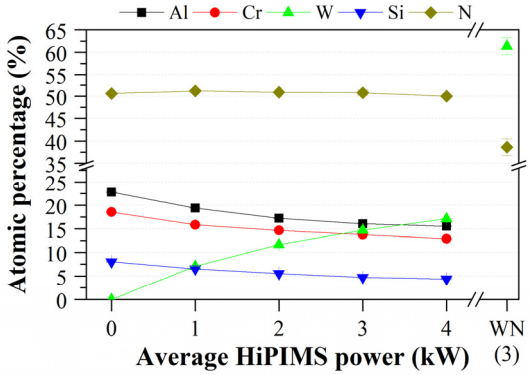

Figure 1. Chemical composition of the films in dependence of the W HiPIMS power.

However, the successive increase of the average HiPIMS power on the W target did not show a linear correlation with the tungsten concentration in the film. In comparison, one of our previous studies showed that increasing the DC power on a Hf cathode during the sputtering of CrAlHfN resulted in an almost linear increase of the Hf content [26]. A similar behavior was revealed during the synthesis of CrAlVN when increasing the DC power on a vanadium target [21]. Thus, the W target on the HiPIMS power supply led to a more irregular sputtering behavior of W atoms when compared to the DC power supplies. Anders et al. explained the W-HiPIMS sputtering by a fluctuating presence of ions at the W target that are accompanied by random ion charges. Due to these various charge exchanges and the relatively low ionization energy of tungsten, deviations in the amount of sputtered W atoms can be explained [27]. When compared to DC, an HiPIMS discharge also results in a larger fraction of both W^+ and W^{2+} ions [18]. Although the Al and Cr proportions slightly decreased with the stepwise tungsten alloying, the Al/Cr ratio (=1.2) remained nearly constant (cf. Table 3). Similar to aluminum and chromium, the silicon content decreased with the incorporations of tungsten, while the nitrogen concentration of all films was approximately 50 at.%.

Table 3. Al/Cr and W/Cr ratios of the AlCrWxSiN films.

W-HiPIMS Power (kW)	0	1	2	3	4
Al/Cr	1.23	1.22	1.17	1.16	1.21
W/Cr	0	0.45	0.80	1.07	1.33

The WN system, which was deposited by means of HiPIMS, exhibited a non-stoichiometric composition of 61.4 ± 1.89 at.% tungsten and 38.6 ± 1.89 at.% nitrogen, suggesting the formation of a tungsten-rich nitride. This result is in correspondence with the results of Baker et al., who revealed that a maximum concentration of 35 at.% N is soluble in a W_2N structure during DC magnetron sputtering. They stated that higher energetic or

bias-assisted processes would be necessary to form stoichiometric WN_x [28]. Thus, the slightly higher nitrogen content of 38.6 ± 1.89 at.% can be attributed to the comparatively higher energetic HiPIMS process. In conclusion, relatively high energies are necessary for the deposition of stoichiometric WN.

The diffractograms in Figure 2 indicate that all systems crystallized in an *fcc* lattice with CrN and WN phases, while *hex* AlN could not be detected. According to Kawate et al. the formation of *hex* AlN can occur for Al/Cr ratios >1.5 [29]. As the Al/Cr ratio of all $AlCrW_xSiN$ films was <1.5, it is concluded that aluminum was dissolved in the *fcc* lattice. Furthermore, no crystalline Si_xN_y phases were detected supposing the formation of an amorphous phase. With increased tungsten contents there was a substantial growth of the peak intensities at 2θ = 37.6°, 43.7°, 63.4°, and 76.1°, i.e., a more textured crystallite structure was developed due to the distinct (111), (200), (202), and (311) orientations of the *fcc* crystals. Similar results are reported in numerous studies, which concern the texture alteration from (111) to a (200) orientation with increasing W contents in sputtered $Cr_{1-x}W_xN_y$ films [4–6]. However, since the cubic CrN, W_2N, and WN lattices are roughly equal in their lattice parameters (CrN = 0.4148 nm, WN = 0.4130 nm, and β-W_2N = 0.4126 nm) [30], superpositions of the reflexes at 2θ = 37.6°, 43.7°, 63.4°, and 76.1° occurred. Chang et al. systematically varied the Cr and W contents in a CrWN system and showed that when exposing the substrates alternately to Cr and W targets with different powers, a stacking of CrN and W_2N nanolayers occurs. Thus, this phenomenon was described as a mixed CrN-W_2N phase with a chemical composition that is dependent on the individual target powers [6]. Similarly, Figure 2 indicates that the intensity and width of the pronounced (111) reflex increased with increasing W HiPIMS powers, suggesting the formation of more tungsten nitrides accompanied by decreased grain sizes. Wu et al. observed a similar behavior when integrating W HiPIMS process in a DC TiAlN deposition. They revealed that a W HiPIMS process increased the compressive stresses and the lattice parameter of TiAlN [17]. Analogously, the increase of the W concentration in $AlCrW_xSiN$ was accompanied by peak shifts of the (111), (202), and (311) reflexes towards lower 2θ angles. These peak shifts can be ascribed to the W HiPIMS procedure, as the diffractogram of the pure WN film also indicated significant shifts of the W_2N reflexes. In particular, when the tungsten content exceeded the chromium content for W > 14.7 at.%, it can be concluded that more W_2N phases were formed leading to a lattice distortion. In this context, Tsai et al. demonstrated that the lattice parameters of CrAlSiN and W_2N differ by about 4.4% [10].

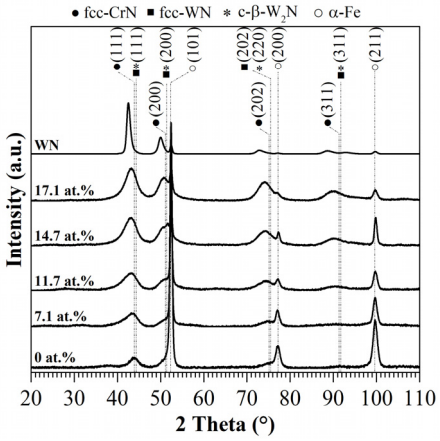

Figure 2. Diffractograms of the as-deposited films in dependence of the W content.

After annealing the films at 500 °C, no substantial changes in the crystallite structure of the $AlCrW_xSiN$ films could be verified (cf. Figure 3). The WN film, however, demonstrated a significant oxidation as a monoclinic WO_3 phase was formed. Zhao et al. also observed an oxygen diffusion, i.e., the formation of WO_3, along the columnar grains of the sputtered WN films after annealing at 500–700 °C for 1 h [31]. Therefore, it is obvious that the W

contents in AlCrW$_x$SiN must have a substantial impact on the oxidation behavior, which will be further discussed in the context of the tribological properties.

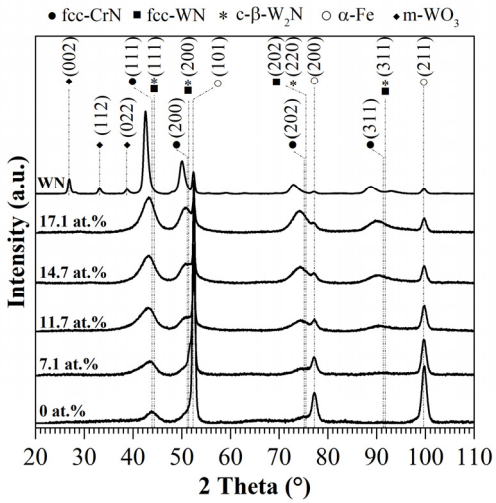

Figure 3. Diffractograms of the films in dependence of the W content after annealing at 500 °C.

3.2. Microstructure

The morphology and topography of the as-deposited films in dependence of the tungsten content are shown in Figure 4. The AlCrSiN film exhibited a columnar film growth and a thickness of 3.42 ± 0.03 µm. With higher average HiPIMS powers on the W target, an increase of the film thicknesses by up to 5.62 ± 0.05 µm was observed. For a tungsten content of 17.1 at.%, however, there was a slight decrease of the film thickness, which could be traced back to the resputtering effects of the enhanced W^+ ion irradiation [17]. When compared to AlCrSiN, the addition of W = 7.1 at.% resulted in the formation of a more needle-shaped structure. According to our previous study, slight Si (~3 at.%) and W (~1.6 at.%) incorporations, which were accompanied by a decrease in the aluminum content, can also result in a significant coarsened columnar growth of AlCrSiWN when compared to AlCrN. It is assumed that tungsten played a significant role in the coarsening of the morphology due to its higher atomic weight [14]. Alloying AlCrSiN with 11.7 to 14.7 at.% tungsten, by contrast, resulted in a clearly denser film growth. This result is in correspondence with the findings of Hones et al., who reported that increasing tungsten contents in $Cr_{1-x}W_xN_y$ changed the morphology from columnar to a more fine-grained structure, which is based on the formation of finer and more randomly orientated crystallites [32]. Therefore, Hones et al. recommend relatively low tungsten additions to CrWN to avoid a film embrittlement [4]. Against this, the $Al_{15.6}Cr_{12.9}W_{17.1}Si_{4.4}N_{50.0}$ film, which is characterized by tungsten exceeding the chromium content, evoked the formation of a slight columnar morphology. The $W_{61.4}N_{38.6}$ film, in turn, exhibited a clear columnar structure.

The diffractograms in Figure 2 disclose that the tungsten induced the formation of a more textured film and increased the tendency to form W_xN_y phases. Based on the findings of Hones et al. [4], the pronounced formation of W_xN_y phases coarsened the film morphology analogously, especially when tungsten exceeded the chromium content (cf. 17.1 at.% W). Thus, it can be concluded that a W content of 11.7 to 14.7 at.% was accompanied by the densest film growth of AlCrW$_x$SiN, which is supposed to bea reason of the balanced W/Cr ratio (Table 3).

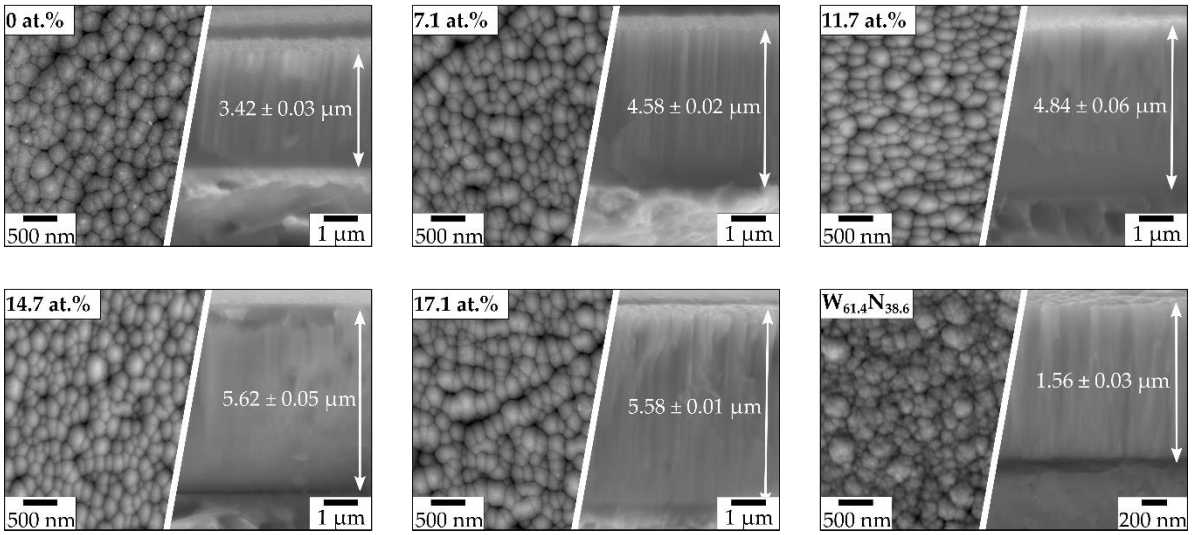

Figure 4. Topography and morphology of the as-deposited films in dependence of the W content.

3.3. Mechanical Properties and Adhesion

Figure 5 reveals an increase of both the hardness and Young's modulus with higher tungsten contents in AlCrW$_x$SiN. The Young's modulus, however, was only marginally increased with higher tungsten concentrations greater than 11.7 at.%. At room temperature, the AlCrSiN system exhibited a relatively low hardness of 19.0 ± 1.5 GPa, while adding 7.1 at.% tungsten resulted in a slight increase of hardness (21.0 ± 1.0 GPa). A hardness ≥24 GPa was obtained when the W/Cr ratio in the films was ≥1 (cf. Table 1), i.e., when the tungsten content exceeded the chromium content and more (200) orientations were formed (Figure 2). Similar to the results of Chang et al., who analyzed CrWN films [6], a pronounced (200) orientation of the *fcc* crystal can account for hardness values >20 GPa. As is known from the literature, the tungsten incorporation in CrWN evokes a phase strengthening effect that is based on more covalent bondings leading to the formation of a solid solution [2,19,33]. Hones et al. explained that when a higher amount of harder WN phases are formed as compared to CrN phases, the hardness is likely to increase. They determined the hardness of WN as 30 ± 1 GPa, while the hardness of CrN was 13 ± 1.5 GPa. However, they concluded that low tungsten additions to CrWN are more beneficial to merge both the hardness of WN as well as the toughness of CrN [4]. Therefore, the hardness and Young's modulus of $W_{61.4}N_{38.6}$ synthesized by HiPIMS (25.8 ± 2.3 GPa) significantly exceeded the mechanical properties of the AlCrW$_x$SiN films (cf. Figure 5). Based on these results, a pronounced texture formation in AlCrW$_x$SiN (cf. Figure 2), which is based on higher W HiPIMS powers, suggested the formation of a CrWN solid solution and comparatively harder W$_x$N$_y$ phases in the films. In this context, Tsai et al. revealed that a CrAlSiN/W_2N superlattice film can decisively increase hardness by up to 40.3 GPa due to a dislocation hindrance [34] and a coherency strain that is generated by a relatively large lattice mismatch (4.4%) of the two-phased film structure [10].

Although an annealing at 500 °C slightly deteriorated the mechanical properties when compared to RT, a tungsten content of 14.7 at.% was still accompanied by a hardness of 20.2 ± 1.4 GPa. Drnovšek et al. investigated the in-situ hardness development of sputtered CrAlSiN (H_{RT} = 37 ± 3 GPa) and revealed a decrease in hardness, with approximately 2 GPa per 100 °C step when annealing up to a temperature of 400 °C. However, after annealing up to 700 °C they observed a hardness comparable to the initial state at RT. The hardness reduction during heating was traced back to lattice vibrations and extensions, which negatively influenced the bondings [35]. Feng et al. also revealed a significant hardness decrease of arc-evaporated AlCrSiWN films after annealing at 700 °C. They traced this behavior back to recrystallization processes which led to a stress relaxation as well as the transformation of phases, e.g., *hex* AlN [20]. However, as the diffractograms

after annealing (Figure 3) did not indicate the formation of new phases, it is likely that dislocation motions reduced the hardness, as explained by Mayrhofer et al. in cases where the annealing temperature was greater than the deposition temperature [36].

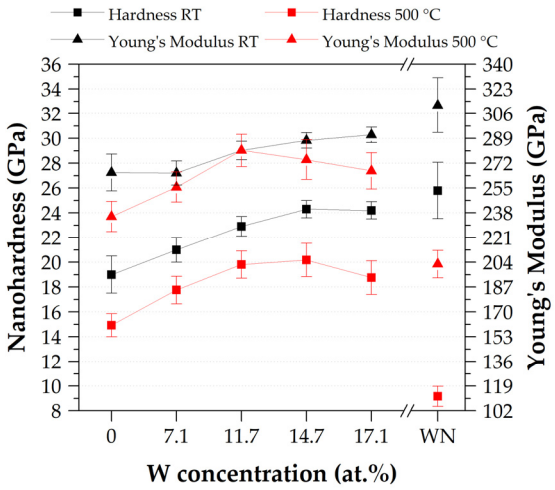

Figure 5. Mechanical properties at room temperature and after annealing.

A tungsten concentration of 17.1 at.% resulted in a slight hardness decrease when compared to W = 14.7 at.%. It is assumed that more WN phases primarily foster a film oxidation and thus a deterioration of the mechanical properties occurs after annealing. The WN film hardness decreased accordingly to 9.16 ± 0.8 GPa, which is based on the formation of m-WO_3 (cf. Figure 3). Hence, a complete deterioration of the WN film was generated after annealing, which is further discussed in context of the tribological properties.

Besides the enhanced mechanical properties, the critical loads (Lc3) of the films in Figure 6 disclosed that the tungsten integration in $AlCrW_xSiN$ had an influence on the film adhesion at RT and after annealing. While the $Al_{22.8}Cr_{18.5}Si_{8.1}N_{50.6}$ film exhibited a relatively low adhesion at RT ($Lc3_{RT}$ = 17.3 ± 1.0 N), which is in correspondence with our previous study [22], the W incorporation led to a considerable increase of the film adhesion. Hones et al. traced the enhanced adhesion of sputtered $Cr_{1-x}W_xN_y$ films back to higher compressive stresses with increased tungsten contents [4]. This result is also in correspondence with the peak shifts shown in Figure 2, suggesting a lattice distortion and stress increase that is induced by the increased W HiPIMS powers. The highest film adhesion was obtained with the $Al_{19.4}Cr_{15.8}W_{7.1}Si_{6.5}N_{51.2}$ system exhibiting a critical load up to 74.7 ± 2.4 N at room temperature and 66.4 ± 1.8 N in the annealed state. When compared to the AlCrSiN reference system, the film adhesion was up to four times higher when alloying with 7.1 at.% tungsten, while it was slightly decreased with further tungsten additions. Similar to the findings of Yau et al. for CrWN, a greater tungsten incorporation resulted in a decrease of film adhesion, which was traced back to higher compressive stresses and an embrittlement [37]. This suggests that the use of relatively low tungsten concentrations (~7.1 at.%) for $AlCrW_xSiN$ systems will maximize the adhesion. In this context, the increasing film thickness with increasing W HiPIMS powers is also an indicator of a slight decrease of the film adhesion. In summary, higher W HiPIMS powers contributed to a hardness increase on the one hand, while the increased film thickness was accompanied by a decreased film adhesion.

3.4. Tribological Properties

The results of the friction behavior in Figure 7 revealed that the gradual tungsten increase in $AlCrW_xSiN$ slightly decreased the coefficient of friction at RT. For $Al_{23}Cr_{19}Si_8N_{51}$, the COF was μ = 0.38 ± 0.06, while an integration of 11.7 to 17.1 at.% tungsten decreased the COF to μ = 0.33 ± 0.03. Tsai et al. analogously compared the friction behavior of a

CrAlSiN monolayer (μ = 0.8) and CrAlSiN/W_2N multilayers (μ~0.6), revealing a decreased coefficient of friction at room temperature due to the integration of W_2N [11].

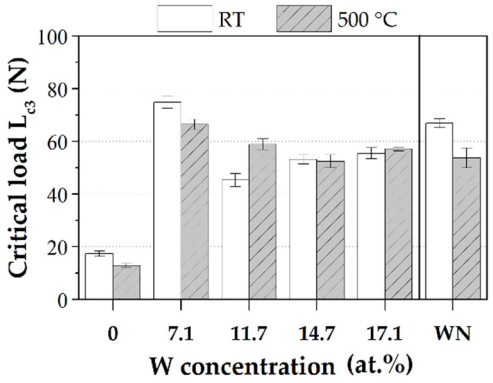

Figure 6. Critical loads (Lc3) at room temperature and after annealing.

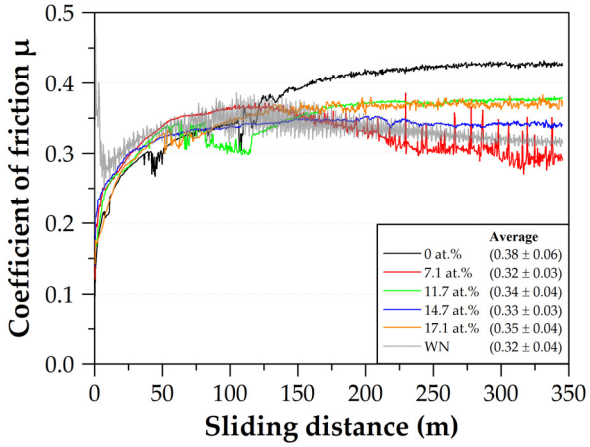

Figure 7. Friction curve profiles and average COFs at room temperature.

From Figures 4 and 7 it can be derived that slight tungsten additions hinder columnar film growth, thus having an impact on the decreased friction at RT. Although the pure $W_{61.4}N_{38.6}$ film exhibited a significantly coarser columnar film growth, the COF of this system (μ = 0.32 ± 0.04) was below the value of AlCrSiN (cf. Figure 7). Thus, the friction of WN cannot be solely attributed to the film morphology but rather to a tribochemical interaction lowering the coefficient of friction. Several studies have proved that an increased tungsten content in CrWN reduces the friction at RT [1,38], which is based on the beginning of a Magnéli phase formation, such as WO_3, that acts as shear structures to evoke a solid lubricating effect [38–40].

Besides pronounced crack formations, the wear track of the WN film in Figure 8f depicts flake-shaped particles with lengths of approximately 2 μm in the center of the tribological contact zone (Spectrum 2), which were found to be local oxidations. Furthermore, these film oxidations were especially pronounced in areas where the WN film formed superficial pores and cracks, which fostered the diffusion of oxygen into the surface through the additional load during the tribometer test. From the COF curves in Figure 7 it can be derived that after a sliding distance of approximately 125 m the effect of tungsten alloying on the reduced friction behavior at RT becomes obvious. This leads to the assumption that this point might indicate the beginning of the aforementioned friction- and force-induced film oxidation.

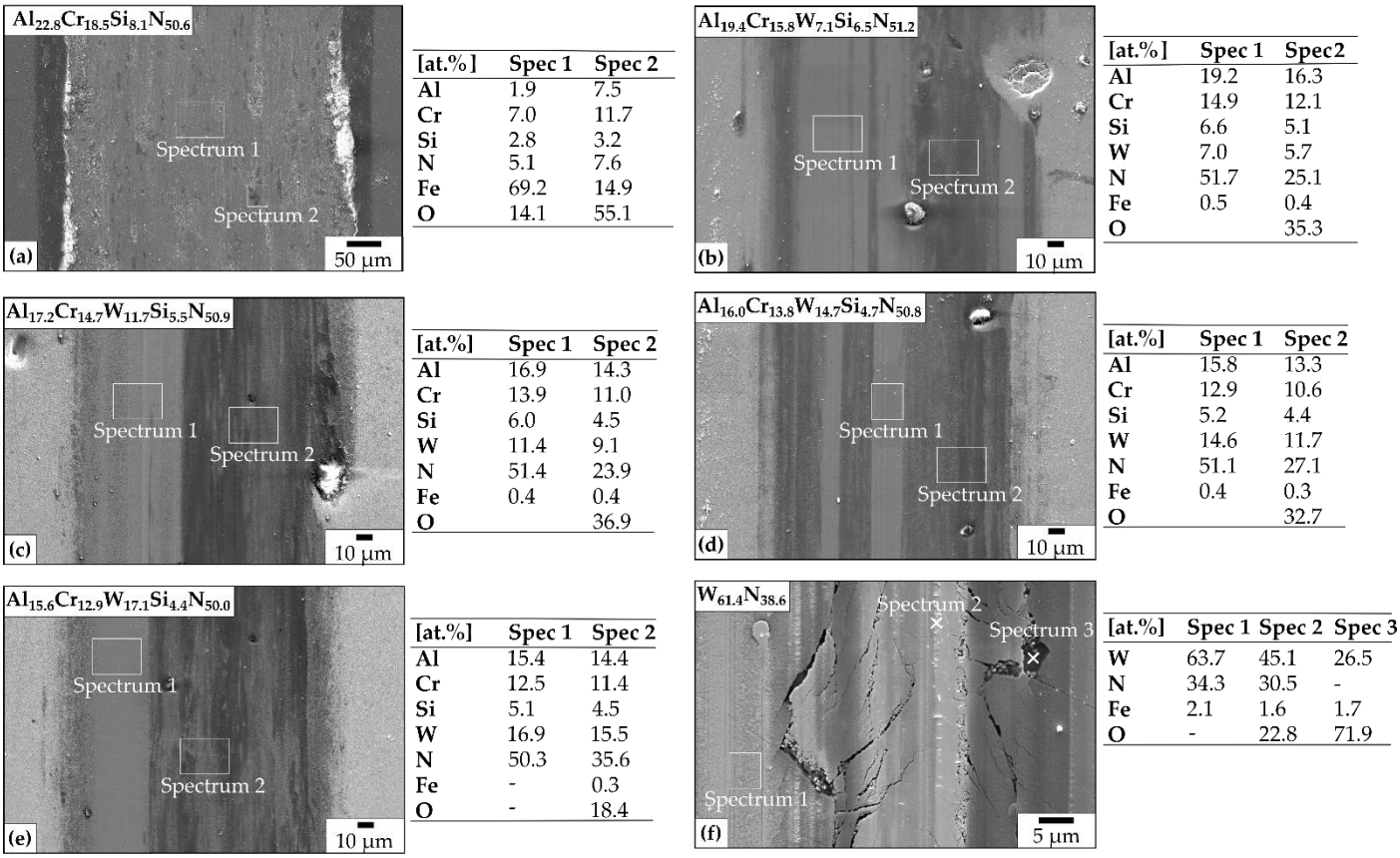

[at.%]	Spec 1	Spec 2
Al	1.9	7.5
Cr	7.0	11.7
Si	2.8	3.2
N	5.1	7.6
Fe	69.2	14.9
O	14.1	55.1

[at.%]	Spec 1	Spec2
Al	19.2	16.3
Cr	14.9	12.1
Si	6.6	5.1
W	7.0	5.7
N	51.7	25.1
Fe	0.5	0.4
O		35.3

[at.%]	Spec 1	Spec 2
Al	16.9	14.3
Cr	13.9	11.0
Si	6.0	4.5
W	11.4	9.1
N	51.4	23.9
Fe	0.4	0.4
O		36.9

[at.%]	Spec 1	Spec 2
Al	15.8	13.3
Cr	12.9	10.6
Si	5.2	4.4
W	14.6	11.7
N	51.1	27.1
Fe	0.4	0.3
O		32.7

[at.%]	Spec 1	Spec 2
Al	15.4	14.4
Cr	12.5	11.4
Si	5.1	4.5
W	16.9	15.5
N	50.3	35.6
Fe	-	0.3
O	-	18.4

[at.%]	Spec 1	Spec 2	Spec 3
W	63.7	45.1	26.5
N	34.3	30.5	-
Fe	2.1	1.6	1.7
O	-	22.8	71.9

Figure 8. EDS analyses of the wear tracks after tribology tests at room temperature.

Similar to the reduced friction with increasing tungsten contents, the wear coefficients at RT were significantly lowered (Figure 9) by a factor of 50. The wear coefficient of AlCrSiN was comparatively high. An explanation for this behavior can be found when considering the wear track of AlCrSiN in Figure 8a, which reveals a complete film delamination and an exposure of the substrate, respectively, due to the relatively high Fe amounts verified by EDS. In contrast to this, the $AlCrW_xSiN$ films were flattened and tended to oxidations and a volatilization of nitrogen, as indicated by the darker areas (Spectrum 2) in Figure 8b–e. These tribochemical interactions are assumed to contribute to a friction reduction, thus leading to a significantly lower wear coefficient of the $AlCrW_xSiN$ systems when compared to AlCrSiN and WN (Figure 9). Furthermore, the integration of both CrN and W_xN_y phases (cf. Figure 2) are assumed to merge properties such as hardness and toughness, as elaborated in [4], resulting in an enhanced adhesion and a better wear resistance at RT.

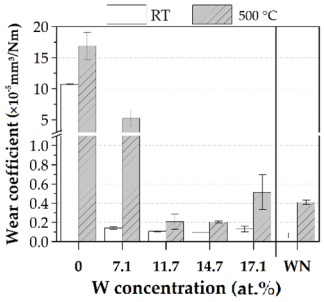

Figure 9. Wear coefficients at room temperature and at 500 °C.

Overall, when compared to room temperature, there was an increase of the coefficient of friction at 500 °C, since the values ranged from $\mu = 0.48 \pm 0.06$ to $\mu = 0.96 \pm 0.11$

(Figure 10). Furthermore, the friction curves in Figure 10 indicate a continuous oscillation after a sliding distance of 25 m. An increase of the friction at 500 °C was also revealed by Mayrhofer et al. for TiAlN/VN superlattice films. However, they did not observe the formation of lubricous oxides at this temperature and explained the increase in friction by a change of abrasive to adhesive wear [41]. In addition, Bobzin et al. observed an increase of the COF of $Cr_{0.53}Al_{0.14}W_{0.33}N$ from 0.5 (RT) to 0.64 (600 °C) when using 100Cr6 (AISI 5210) as a counterpart. They concluded that the friction increase is a result of the high oxidation temperature of tungsten, thus no substantial friction reduction is created [42,43]. Furthermore, increased tungsten concentrations in CrWN can result in an increased surface roughness and a pronounced formation of Cr_2O_3 [2,44]. Huang et al., for instance, concluded that WO_3, Cr_2O_3, and $CrWO_4$ phases formed in CrWN after annealing at 650 °C in air [38]. A comparison of Figures 2 and 3, however, reveals no phase transformations of the $AlCrW_xSiN$ film surfaces after annealing at 500 °C, pointing out that the tribological mechanisms fostered the increase in friction.

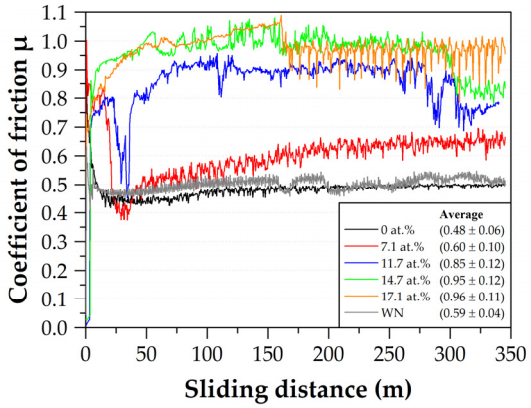

Figure 10. Friction curve profiles and average COFs at 500 °C.

As the COF increased at 500 °C, the wear coefficient was also approximately two times higher when compared to RT. However, W concentrations between 11.7–14.7 at.% were associated with the lowest wear coefficient (~0.2 × 10^{-5} mm^3/Nm) at high temperatures (Figure 9). A closer look at the $AlCrW_xSiN$ wear tracks, which had tribological contact at 500 °C in Figure 11b–e, revealed a structural, squamous alteration of the film topography in dependence of the direction of rotation. On the one hand, several areas retained the initial film composition with slight oxidations, and on the other hand, scaly areas having a darker appearance exhibited a notable oxygen content followed by a depletion of nitrogen. Furthermore, oxidized sections were accompanied by a local increase of the surface roughness, which explained the increasing and alternating friction behavior at 500 °C shown in Figure 10. Films with a W content >11.7 at.% tended to slight crack formations in the wear track through which the oxygen diffusion was promoted. These cracks were likely to form as a result of the comparatively brittle W_xN_y phases indicated in Figure 2. According to Figure 11d, the nearly balanced W/Cr ratio in $Al_{16.0}Cr_{13.8}W_{14.7}Si_{4.7}N_{50.9}$ resulted in a slightly lower oxidation rate when compared to the other film systems. As the amount of oxidized areas in the wear track was further increased with the tungsten content, it can be concluded that tungsten primarily fostered the oxidation during tribological contacts at 500 °C. The high temperature tribological contact of the $W_{61.4}N_{38.6}$ film in Figure 11f verified a film oxidation. On the one hand, an oxygen-rich tribofilm was developed on the WN film (Spectrum 1), while on the other hand, a complete oxidation of tungsten took place in areas of abrasive wear debris. According to the chemical composition determined by EDS in combination with the XRD results after annealing (Figure 3), it was obvious that these tungsten oxides complied with the WO_3 phase. As this WO_3 phase was already apparent after the sole annealing at 500 °C, it is obvious that the tribological contact additionally fostered the oxidation through the abrasive wear debris, which is initiated

by crack formations of the oxidized WN film (Figure 11f—Spectrum 1). Based on the superficial outbreaks in the wear track of the WN film, the COF at 500 °C ($\mu = 0.59 \pm 0.04$) was higher when compared to room temperature ($\mu = 0.32 \pm 0.04$). A study of Gassner et al. showed that sliding Al_2O_3 against WN also resulted in an increase of the coefficient of friction from $\mu = 0.3$ (RT) to $\mu = 0.5$ (at 500 °C), which was attributed to an increase in the surface roughness. However, they did not detect oxide phases by means of XRD for this temperature. Tribometer tests at 700 °C in turn resulted in a decrease of the COF to μ~0.45 due to the formation of W_xO_y Magnéli phases acting as a lubricant [45].

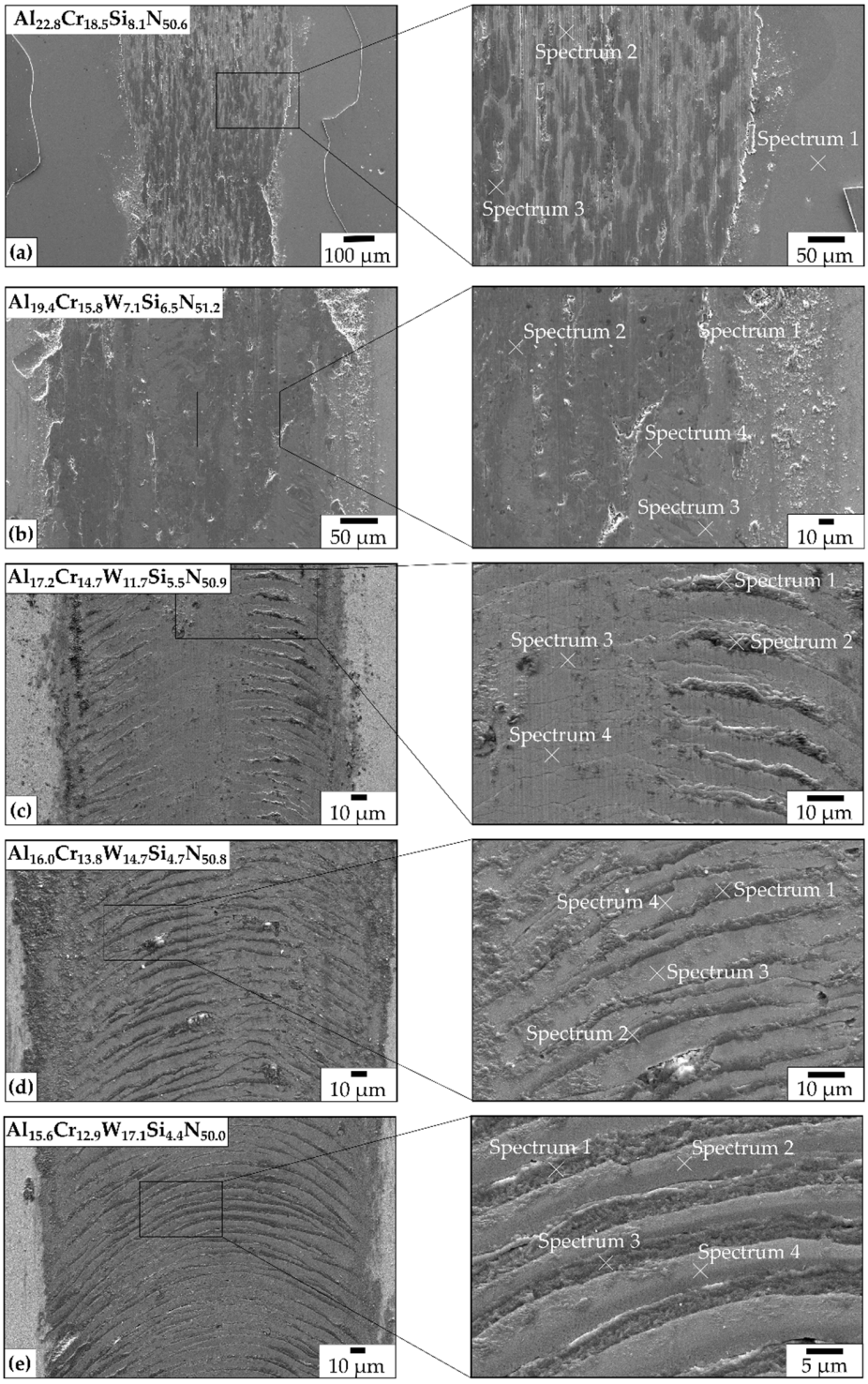

[at.%]	Spec 1	Spec 2	Spec 3
Al	0.1	1.3	0.5
Cr	36.5	5.9	2.6
Si	1.6	1.8	1.0
N	0.2	-	3.7
Fe	61.4	35.1	27.3
O	-	55.8	64.8

[at.%]	Spec 1	Spec 2	Spec 3	Spec 4
Al	6.2	7.0	18.4	21.3
Cr	4.5	6.7	13.8	15.7
Si	1.7	2.0	6.0	6.0
W	2.0	2.5	6.7	8.0
N	1.2	1.9	46.9	44.7
Fe	16.2	15.6	0.8	1.2
O	68.2	64.5	7.4	3.3

[at.%]	Spec 1	Spec 2	Spec 3	Spec 4
Al	13.3	11.0	16.9	18.7
Cr	9.2	6.1	14.1	15.2
Si	2.2	1.9	5.2	5.4
W	6.0	4.4	11.4	12.7
N	2.1	6.6	48.2	44.8
O	67.3	70.1	4.3	3.3

[at.%]	Spec 1	Spec 2	Spec 3	Spec 4
Al	12.6	12.6	15.1	14.8
Cr	10.1	10.4	12.3	12.6
Si	3.6	3.8	3.9	4.2
W	11.3	11.3	13.8	13.7
N	4.3	16.1	41.5	37.7
O	57.7	45.5	13.2	16.6

[at.%]	Spec 1	Spec 2	Spec 3	Spec 4
Al	11.3	15.4	9.4	16.0
Cr	8.5	13.4	7.0	13.0
Si	2.3	4.6	2.2	4.1
W	11.8	16.8	10.0	17.3
N	-	44.2	5.8	45.8
O	66.7	5.6	65.7	3.8

Figure 11. *Cont.*

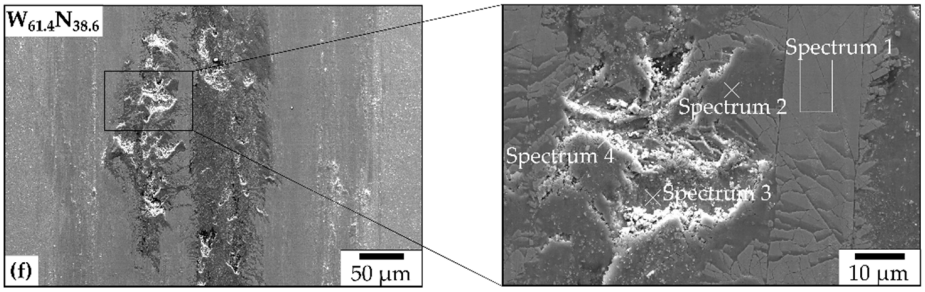

[at.%]	Spec 1	Spec 2	Spec 3	Spec 4
W	37.0	22.6	22.0	29.8
N	16.1	-	-	-
Fe	-	-	5.0	4.4
O	46.9	77.4	73.0	65.9

Figure 11. EDS analyses of the wear tracks after tribology tests at 500 °C.

A contextualization of the cited findings with the COF values shown in Figure 10 leads to the conclusion that a temperature of 500 °C induces the formation of WO_3 on the WN film, which, however, does not contribute to a friction reduction due to the wear debris verified in Figure 11f. Although the friction of the $AlCrW_xSiN$ systems at 500 °C was increased with higher W contents, the wear coefficient was significantly decreased for W contents between 11.7–14.7 at.%. A tungsten content of 17.1 at.% in turn slightly increased the wear rate due to the formation of more and broader squamous oxidized areas in the wear track. Finally, the $W_{61.4}N_{38.6}$ film disclosed that the tungsten nitride phase was primarily oxidized, based on the non-stoichiometric composition. Due to the balanced W/Cr ratio (see Table 3), a higher hardness and the lower wear was revealed for $Al_{17.2}Cr_{14.7}W_{11.7}Si_{5.5}N_{50.9}$ and $Al_{16.0}Cr_{13.8}W_{14.7}Si_{4.7}N_{50.9}$. In particular, a balanced W/Cr ratio was accompanied by a slightly lower oxidation rate after tribological contact at 500 °C.

4. Conclusions

A DC hybrid magnetron sputtering process integrating a W-HiPIMS supply was firstly applied to synthesize $AlCrW_xSiN$ films with varying tungsten contents (0–17.1 at.%). The tungsten incorporation significantly influenced the crystallographic and microstructural properties, leading to positively affected tribomechanical properties at room and high temperatures (500 °C) through slight W additions. The main findings obtained enabled us to draw the following conclusions:

- The HiPIMS supply to the W target generated a non-stoichiometric $W_{61.4}N_{38.6}$, which formed an m-WO_3 phase after annealing at 500 °C and deteriorated the mechanical properties. In contrast to this, the $AlCrW_xSiN$ film surfaces did not exhibit any crystalline phase transformations after the heat treatment.
- The successive increase of W in $AlCrSiW_xN$ resulted in a denser film growth and steadily increased the film hardness, thus further enhancing the film adhesion.
- Based on the denser film growth, tungsten additions to $AlCrW_xSiN$ resulted in slight decrease of the COF at room temperature. In particular, the formation of cracks in the WN wear track fostered oxygen diffusion at room temperature. Thus, a preliminary stage in the formation of friction-reducing tungsten oxides begun, which is of interest for further research.
- It was shown that at 500 °C higher tungsten proportions led to a significantly increased and alternating friction behavior due to scaly oxidations in the wear tracks, which locally increased the surface roughness in the wear track. Furthermore, the WN film exhibited a fracturing in the wear track, which increased the friction. Additionally, the partial transformation of WN to m-WO_3 did not induce a self-lubricating effect. Therefore, the friction was generally increased at 500 °C for all systems.
- Although the friction and oxidation in the wear track were intensified at high temperatures, the wear coefficient was significantly decreased for films with a balanced W/Cr ratio. This finding offers great potential for tungsten as an alloying element in chromium-based systems for use as wear resistant film.

Future investigations should consider the tribological behavior of AlCrWSiN films at temperatures higher than 500 °C and on substrates with a higher temperature resistance,

such as cemented carbide. It is believed that the oxide formations at RT and 500 °C are a preliminary step in the complex formation of lubricating Magnéli phases. Therefore, higher temperatures would be necessary to induce a self-lubricating effect, which reduces the friction of AlCrWSiN for high temperature applications like hard metal cutting.

Author Contributions: Conceptualization, A.F.; Methodology, A.F.; Validation, W.T., D.S., and A.F.; Investigation, A.F.; Writing—Original Draft Preparation, A.F.; Writing—Review and Editing, W.T. and D.S.; Visualization, A.F.; Supervision, W.T.; Project Administration, W.T. and A.F.; Funding Acquisition, W.T. All authors have read and agreed to the published version of the manuscript.

Funding: We would like to express our special thanks to the German Research Foundation (DFG) for funding the project TI 343/151–1 "Investigation of the mechanisms during sintering process modifications of multi-component sputter materials and the phase specific deposition of AlCrSi (W, Ta) N". Furthermore, we acknowledge financial support by Deutsche Forschungsgemeinschaft and Technische Universität Dortmund/TU Dortmund University within the funding program Open Access Publishing.

Institutional Review Board Statement: Not applicable.

Informed Consent Statement: Not applicable.

Conflicts of Interest: The authors declare no conflict of interest.

References

1. Wu, W.-Y.; Wu, C.-H.; Xiao, B.-H.; Yang, T.-X.; Lin, S.-Y.; Chen, P.-H.; Chang, C.-L. Microstructure, mechanical and tribological properties of CrWN films deposited by DC magnetron sputtering. *Vacuum* **2013**, *87*, 209–212. [CrossRef]
2. Lin, T.-N.; Han, S.; Weng, K.-W.; Lee, C.-T. Investigation on the structural and mechanical properties of anti-sticking sputtered tungsten chromium nitride films. *Thin Solid Films* **2013**, *529*, 333–337. [CrossRef]
3. Yao, S.H.; Su, Y.L.; Kao, W.H. Effect of Ag/W addition on the wear performance of CrN coatings prepared by RF unbalanced magnetron sputtering. *Mat. Sci. Eng. A* **2005**, *398*, 88–92. [CrossRef]
4. Hones, P.; Consiglio, R.; Randall, N.; Lévy, F. Mechanical properties of hard chromium tungsten nitride coatings. *Surf. Coat. Technol.* **2000**, *125*, 179–184. [CrossRef]
5. Chen, Y.-I.; Cheng, Y.-R.; Chang, L.-C.; Lee, J.-W. Chemical inertness of Cr–W–N coatings in glass molding. *Thin Solid Films* **2015**, *593*, 102–109. [CrossRef]
6. Chang, L.-C.; Zheng, Y.-Z.; Gao, Y.-X.; Chen, Y.-I. Mechanical properties and oxidation resistance of sputtered Cr–W–N coatings. *Surf. Coat. Technol.* **2017**, *320*, 196–200. [CrossRef]
7. Polcar, T.; Cavaleiro, A. High-temperature tribological properties of CrAlN, CrAlSiN and AlCrSiN coatings. *Surf. Coat. Technol.* **2011**, *206*, 1244–1251. [CrossRef]
8. Tien, S.-K.; Lin, C.-H.; Tsai, Y.-Z.; Duh, J.-G. Effect of nitrogen flow on the properties of quaternary CrAlSiN coatings at elevated temperatures. *Surf. Coat. Technol.* **2007**, *202*, 735–739. [CrossRef]
9. Chang, C.-C.; Chen, H.-W.; Lee, J.-W.; Duh, J.-G. Development of Si-modified CrAlSiN nanocomposite coating for anti-wear application in extreme environment. *Surf. Coat. Technol.* **2015**, *284*, 273–280. [CrossRef]
10. Tsai, Y.Z.; Duh, J.G. Enhanced hardness of CrAlSiN/W_2N superlattice coatings deposited by direct current magnetron sputtering. *J. Mater. Res.* **2010**, *25*, 2325–2329. [CrossRef]
11. Tsai, Y.-Z.; Duh, J.-G. Tribological behavior of CrAlSiN/W_2N multilayer coatings deposited by DC magnetron sputtering. *Thin Solid Films* **2010**, *518*, 7523–7526. [CrossRef]
12. Chan, Y.-C.; Chen, H.-W.; Tsai, Y.-Z.; Duh, J.-G.; Lee, J.-W. Texture, microstructure and anti-wear characteristics in isostructural CrAlSiN/W_2N multilayer coatings. *Thin Solid Films* **2013**, *544*, 265–269. [CrossRef]
13. Tillmann, W.; Fehr, A.; Stangier, D. Microstructural and tribological properties of sputtered AlCrSiWN films deposited with segmented powder metallurgic target materials. *Thin Solid Films* **2019**, *687*, 137465. [CrossRef]
14. Tillmann, W.; Fehr, A.; Stangier, D. Powder metallurgic fabricated plug targets for the synthesis of AlCrSiWN multicomponent coating systems. *Int J. Refract. Met. H.* **2019**, *85*, 105081. [CrossRef]
15. Hones, P.; Martin, N.; Regula, M.; Lévy, F. Structural and mechanical properties ofchromium nitride, molybdenum nitride, and tungsten nitride thin films. *J. Phys. D Appl. Phys.* **2003**, *36*, 1023–1029. [CrossRef]
16. Velicu, I.-L.; Tiron, V.; Porosnicu, C.; Burducea, I.; Lupu, N.; Stoian, G.; Popa, G.; Munteanu, D. Enhanced properties of tungsten thin films deposited with a novel HiPIMS approach. *Appl. Surf. Sci.* **2017**, *424*, 397–406. [CrossRef]
17. Wu, Z.; Tengstrand, O.; Bakhit, B.; Lu, J.; Greene, J.E.; Hultman, L.; Petrov, I.; Greczynski, G. Growth of dense, hard yet low-stress Ti 0.40 Al 0.27 W 0.33 N nanocomposite films with rotating substrate and no external substrate heating. *J. Vac. Sci. Technol. A* **2020**, *38*, 23006. [CrossRef]
18. Tiron, V.; Velicu, I.-L.; Porosnicu, C.; Burducea, I.; Dinca, P.; Malinský, P. Tungsten nitride coatings obtained by HiPIMS as plasma facing materials for fusion applications. *Appl. Surf. Sci.* **2017**, *416*, 878–884. [CrossRef]

19. Yang, J.F.; Prakash, B.; Yuan, Z.G.; Jiang, Y.; Wang, X.P.; Fang, Q.F. Influence of sputtering target power on microstructure and mechanical properties of W-N and Ta-N coatings. *Nanosci. Nanotechnol. Lett.* **2012**, *4*, 604–608. [CrossRef]
20. Feng, Y.-P.; Zhang, L.; Ke, R.-L.; Wan, Q.-L.; Wang, Z.; Lu, Z.-H. Thermal stability and oxidation behavior of AlTiN, AlCrN and AlCrSiWN coatings. *Int J. Refract. Met. H.* **2014**, *43*, 241–249. [CrossRef]
21. Tillmann, W.; Kokalj, D.; Stangier, D.; Paulus, M.; Sternemann, C.; Tolan, M. Investigation of the influence of the vanadium content on the high temperature tribo-mechanical properties of DC magnetron sputtered AlCrVN thin films. *Surf. Coat. Technol.* **2017**, *328*, 172–181. [CrossRef]
22. Tillmann, W.; Fehr, A.; Stangier, D.; Dildrop, M. Influences of substrate pretreatments and Ti/Cr interlayers on the adhesion and hardness of CrAlSiN and TiAlSiN films deposited on Al_2O_3 and ZrO_2-$8Y_2O_3$ thermal barrier coatings. *Results Phys.* **2019**, *12*, 2206–2212. [CrossRef]
23. Tillmann, W.; Fehr, A.; Stangier, D.; Dildrop, M.; Homberg, W.; Lossen, B.; Hijazi, D. Al_2O_3/ZrO_2-$8Y_2O_3$ and (Cr,Ti)AlSiN tool coatings to influence the temperature and surface quality in friction-spinning processes. *Prod. Eng.* **2019**, *13*, 449–457. [CrossRef]
24. Oliver, W.C.; Pharr, G.M. An improved technique for determining hardness and elastic modulus using load and displacement sensing indentation experiments. *J. Mater. Res.* **1992**, *7*, 1564–1583. [CrossRef]
25. *ASTM C1624–05 Standard Test Method for Adhesion Strength and Mechanical Failure Modes of Ceramic Coatings by Quantitative Single Point Scratch Testing*; ASTM: West Conshohocken, PA, USA, 2005.
26. Tillmann, W.; Lopes Dias, N.F.; Stangier, D. Effect of Hf on the microstructure, mechanical properties, and oxidation behavior of sputtered CrAlN films. *Vacuum* **2018**, *154*, 208–213. [CrossRef]
27. Anders, A.; Andersson, J.; Ehiasarian, A. High power impulse magnetron sputtering: Current-voltage-time characteristics indicate the onset of sustained self-sputtering. *J. Appl. Phys.* **2007**, *102*, 113303. [CrossRef]
28. Baker, C.C.; Shah, S.I. Reactive sputter deposition of tungsten nitride thin films. *J. Vac. Sci. Technol. A Vac. Surf. Film.* **2002**, *20*, 1699–1703. [CrossRef]
29. Kawate, M.; Kimura, A.; Suzuki, T. Microhardness and lattice parameter of $Cr_{1-x}Al_xN$ films. *J. Vac. Sci. Technol. A* **2002**, *20*, 569–571. [CrossRef]
30. Tsai, Y.-Z.; Duh, J.-G. Thermal stability and microstructure characterization of CrN/WN multilayer coatings fabricated by ion-beam assisted deposition. *Surf. Coat. Technol.* **2005**, *200*, 1683–1689. [CrossRef]
31. Zhao, H.; Yu, L.; Ye, F. Comparison study on the oxidation behavior of WN and WCN ceramic coatings during heat treatment. *Mater. Chem. Phys.* **2018**, *206*, 144–149. [CrossRef]
32. Hones, P.; Diserens, M.; Sanjinés, R.; Lévy, F. Electronic structure and mechanical properties of hard coatings from the chromium–tungsten nitride system. *J. Vac. Sci. Technol. B* **2000**, *18*, 2851–2856. [CrossRef]
33. Endrino, J.L.; Derflinger, V. The influence of alloying elements on the phase stability and mechanical properties of AlCrN coatings. *Surf. Coat. Technol.* **2005**, *200*, 988–992. [CrossRef]
34. Chu, X.; Barnett, S.A. Model of superlattice yield stress and hardness enhancements. *J. Appl. Phys.* **1995**, *77*, 4403–4411. [CrossRef]
35. Drnovšek, A.; Rebelo de Figueiredo, M.; Vo, H.; Xia, A.; Vachhani, S.J.; Kolozsvári, S.; Hosemann, P.; Franz, R. Correlating high temperature mechanical and tribological properties of CrAlN and CrAlSiN hard coatings. *Surf. Coat. Technol.* **2019**, *372*, 361–368. [CrossRef]
36. Mayrhofer, P.H.; Mitterer, C.; Hultman, L.; Clemens, H. Microstructural design of hard coatings. *Prog. Mater Sci.* **2006**, *51*, 1032–1114. [CrossRef]
37. Yau, B.-S.; Chu, C.-W.; Lin, D.; Lee, W.; Duh, J.-G.; Lin, C.-H. Tungsten doped chromium nitride coatings. *Thin Solid Films* **2008**, *516*, 1877–1882. [CrossRef]
38. Huang, X.; Xie, Z.; Li, K.; Chen, Q.; Gong, F.; Chen, Y.; Feng, B.; Hu, S.; Chen, Y.; Han, B.; et al. Microstructure, wear and oxidation resistance of CrWN glass molding coatings synthesized by plasma enhanced magnetron sputtering. *Vacuum* **2020**, *174*, 109206. [CrossRef]
39. Reeswinkel, T.; Music, D.; Schneider, J.M. Coulomb-potential-dependent decohesion of Magnéli phases. *J. Phys. Condens. Matter* **2010**, *22*, 292203. [CrossRef] [PubMed]
40. Ju, H.; Ding, N.; Xu, J.; Yu, L.; Asempah, I.; Xu, J.; Yi, G.; Ma, B. Crystal structure and the improvement of the mechanical and tribological properties of tungsten nitride films by addition of titanium. *Surf. Coat. Technol.* **2018**, *345*, 132–139. [CrossRef]
41. Mayrhofer, P.H.; Hovsepian, P.E.; Mitterer, C.; Münz, W.-D. Calorimetric evidence for frictional self-adaptation of TiAlN/VN superlattice coatings. *Surf. Coat. Technol.* **2004**, *177*, 341–347. [CrossRef]
42. Bobzin, K.; Bagcivan, N.; Ewering, M.; Brugnara, R.H.; Theiß, S. DC-MSIP/HPPMS (Cr,Al,V)N and (Cr,Al,W)N thin films for high-temperature friction reduction. *Surf. Coat. Technol.* **2011**, *205*, 2887–2892. [CrossRef]
43. Lugscheider, E.; Knotek, O.; Bobzin, K.; Bärwulf, S. Tribological properties, phase generation and high temperature phase stability of tungsten- and vanadium-oxides deposited by reactive MSIP-PVD process for innovative lubrication applications. *Surf. Coat. Technol.* **2000**, *133–134*, 362–368. [CrossRef]
44. Lin, C.-H.; Duh, J.-G.; Yau, B.-S. Processing of chromium tungsten nitride hard coatings for glass molding. *Surf. Coat. Technol.* **2006**, *201*, 1316–1322. [CrossRef]
45. Gassner, G.; Mayrhofer, P.H.; Kutschej, K.; Mitterer, C.; Kathrein, M. Magnéli phase formation of PVD Mo–N and W–N coatings. *Surf. Coat. Technol.* **2006**, *201*, 3335–3341. [CrossRef]